Molecular Vision 2022; 28:230-244 <http://www.molvis.org/molvis/v28/230>
Received 11 January 2021 | Accepted 17 August 2022 | Published 19 August 2022

Untargeted metabolomic analysis of aqueous humor in diabetic macular edema

Kai On Chu,[1,2] Tina InLam Chan,[1] Kwok Ping Chan,[1] Yolanda WongYing Yip,[1] Malini Bakthavatsalam,[1] Chi Chiu Wang,[2,3,4] Chi Pui Pang,[1] Marten E. Brelen[1]

[1]Department of Ophthalmology and Visual Sciences, the Chinese University of Hong Kong; [2]Department of Obstetrics and Gynaecology, the Chinese University of Hong Kong; [3]Li Ka Shing Institute of Health Science, the Chinese University of Hong Kong; [4]School of Biomedical Sciences, the Chinese University of Hong Kong

Background: The mechanism of diabetic macular edema (DME) was explored by comparing the intraocular metabolite profiles of the aqueous humor of patients with DME to those of diabetic patients without DME using untargeted metabolomic analysis.

Methods: Aqueous samples from 18 type 2 diabetic patients with DME and 18 type 2 diabetic patients without DME used as controls were analyzed using liquid chromatography–mass spectrometry (LCMS). The two groups of patients were age and gender matched and had no systemic diseases other than diabetes mellitus (DM). The metabolites were analyzed using orthogonal partial least square discriminant analysis.

Results: The metabolite profiles in DME patients differed from those in DM controls. This indicates the following metabolic derangements in DME: (a) a higher amount of oxidized fatty acids but a lower amount of endogenous antioxidants (oxidative stress); (b) higher levels of β-glucose and homocysteine but a lower level of sorbitol (hyperglycemia); (c) a higher amount of prostaglandin metabolites (inflammation); (d) higher amounts of acylcarnitines, odd-numbered fatty acids, and 7,8-diaminononanoate (respiration deterioration); (e) a higher amount of neurotransmitter metabolites and homovanillic acid (neuronal damage); (f) a lower amount of extracellular matrix (ECM) constituents (ECM deterioration); and (g) a higher amount of di-amino peptides (microvascular damage).

Conclusions: The change in the metabolic profiles in the aqueous humor of DME patients compared to DM controls without DME indicates that DME patients may have less capability to resist various stresses or damaging pathological conditions, such as oxidative stress, mitochondrial insufficiency, inflammation, and ECM deterioration.

Diabetic macular edema (DME) is a common sight-threatening complication of diabetic retinopathy (DR) affecting 15% of all diabetic patients within the first 15 years of diagnosis. The mechanism of DME is complex and poorly understood but is believed to involve multifactorial processes of vascular dysfunction, oxidative stress, and inflammation [1,2]. These pathogenic conditions lead to the activation of glial cells and the subsequent migration of microglial cells into the sub-retinal space [3]. With the loss of homeostatic functions, the Muller cells become swollen due to water retention [4] and the inner nuclear layer becomes damaged. Subsequently, the tight junction of retinal pigment epithelial cells is disrupted, affecting barrier properties [5,6]. The choroidal capillaries become more permeable due to the loss of pericytes and microglial cells. As a result, the dysregulation of fluid and transport proteins in the intercellular space lead to fluid accumulation and edema in the sub-retinal space of the macula [7,8]. Complicated by immature neovascularization, an intraocular vicious cycle of fluid retention occurs [8].

In diabetic patients, metabolic disruptions in tissue cells can lead to derangements in metabolic pathways, including the polyol, advanced glycation end product, protein kinase C, and hexosamine pathways [9]. In the eye, there can be retinal pericyte apoptosis, rectifying potassium channel Kir4.1 and the water channel aquaporin 4 dysfunction, [10] destabilization of the tight junction barrier due to oxidative stress [11], and inflammation [12]. Metabolic changes have been found intraocularly, such as elevated lactate and glycolytic intermediates and depletion of ascorbic acid and free cytosolic NADPH in the vitreous humor [13-15]. Diabetic patients with and without DME can have intraocular metabolite profile changes.

The eye is a discrete system with a blood–aqueous and a blood–retinal barrier separating it from the systemic circulation. The exchange of biochemical substances across the compartments is dependent on active and selective

Correspondence to: Marten E. Brelen, Department of Ophthalmology and Visual Sciences The Chinese University of Hong Kong, Hong Kong Eye Hospital, 147K, Argyle Street, Kowloon, Hong Kong; Phone: (852) 39433806; FAX: (852) 27159490; email: marten.brelen@cuhk.edu.hk

transportation of molecules, such as nutrients and metabolites. However, the collection of retinal tissues for metabolomic analysis is invasive and clinically not possible. Although vitreous humor can be accessible, the humor collection imposes risks, such as vitreous hemorrhage, retinal tears, and detachment. However, aqueous humor can be readily obtained before anti-vascular endothelial growth factor (VEGF) agent injection or during cataract surgery in diabetes mellitus (DM) patients. Therefore, we chose to use aqueous humor for this metabolomic study.

The aqueous humor contains mediators, including nutrients and metabolites, to maintain homeostasis of the eye. Its composition can reflect pathophysiological changes in the retina [15]. Because aqueous humor is secreted by epithelial-lined ciliary processes in the posterior chamber, its composition can correlate with the vitreous humor [16], which is the reservoir containing metabolic molecules released from the retina. Many reported studies have used aqueous humor for metabolomic and proteomic investigations of posterior segment disorders, such as age-related macular disorder [17,18], DR [19], and central retinal vein occlusion [20]. In this study, we used untargeted metabolomics to explore the metabolite profiles of aqueous humor in diabetic patients with and without DME. To ensure a broad-spectrum coverage of metabolites, we used reverse-phase liquid chromatography-mass spectrometry (RPLC-MS) and hydrophilic interaction liquid chromatography-mass spectrometry (HILIC-MS) with both positive and negative electrospray ionization (ESI). Authentic chemical standards were used to validate the identified metabolite molecules.

METHODS

Subjects: Aqueous humor samples were obtained from 18 type 2 diabetic patients with DME and 18 type 2 DM patients without DME while undergoing phacoemulsification surgery. The two groups of patients were age and gender matched, and all patients were without systemic diseases other than DM. Aqueous humor samples were taken using a 25-gauge needle inserted through a 1 mm paracentesis made in the peripheral cornea in the mid anterior chamber. Approximately 100 µl aqueous humor was biopsied, transferred to a 500 µl centrifugal vial, and immediately frozen in dry ice before storage at −80 °C until analysis.

This study was approved by the Ethics Committees of the Kowloon Central Kowloon East (KCKE) Cluster and the New Territories East Cluster (NTECT) of the Hospital Authority, Hong Kong. The study protocol adhered to the tenets of the Declaration of Helsinki. Patients or their legal guardians consented to the use of their clinical data for research purposes.

Aqueous humor samples preparation: For RPLC-MS analysis, a 100 µl acetonitrile/methanol (1:1) mixture was mixed with 25 µl aqueous humor for centrifugation at 600 ×g for 15 min at 4 °C. The supernatant was vortexed for 30 s, frozen in liquid nitrogen for 1 min, thawed at room temperature for 5 min, and sonicated for 10 min. This procedure was repeated twice. After further centrifugation for 10 min at 16,200 ×g, the supernatant was pipetted into a 1 ml high-performance liquid chromatography (HPLC) vial for vacuum drying and re-dissolved into 50 µl 20% acetonitrile. After further centrifugation at 16,200 ×g for 10 min at 4 °C, the supernatant was transferred into an HPLC vial for analysis or stored at −80 °C until analysis.

For HILIC-MS analysis, a 100 µl acetonitrile/methanol (1:1) mixture was mixed with 25 µl aqueous humor for centrifugation at 600 ×g for 15 min at 4 °C. It was subsequently vortexed for 30 s, sonicated for 10 min, and centrifuged for 15 min at 16,200 ×g at 4 °C. The supernatant was pipetted into a centrifuge vial. The extraction was repeated twice and pooled. The mixture was stored at −20 °C for an hour and then centrifuged at 16,200 ×g for 15 min at 4 °C. The supernatant was evaporated to dryness by Speedvac. The residue was dissolved in 50 µl 70% acetonitrile and sonicated for 10 min. After centrifugation for 15 min at 16,200 xg at 4 °C, the supernatant was transferred into an HPLC glass vial for LCMS analysis or stored at −80 °C.

Metabolomics analysis: For hydrophobic analysis, a nano ultra-performance liquid chromatography system (ACQUITY Nano UPLC M-Class System, Waters Corporation, Milford, MA) was used. Reverse-phase separation by a 75 µm × 250 mm × 1.7 µm BEH130 C18 column (Waters Corporation) was performed at 45 °C, and 1 µl was injected; the flow rate was at 0.5µl/min. Gradient elution was performed with mobile phase A (5% (v/v) acetonitrile in 0.2% acetic acid) and mobile phase B (95% (v/v) acetonitrile in 0.2% acetic acid). The gradient duration was 35.5 min. Binary gradient elution was from 0–1.34 min, 95% A; 1.34–15.0 min, 80% A; 15.0–18.5 min, 45% A; 18.5–20.5 min, 20% A; 20.5–30.5 min, 20% A; 30.5–32.5 min, 95% A; and 32.5–35.5 min, 95% A.

For hydrophilic analysis, a micro HPLC system (Agilent 1100 micro HPLC system, Santa Clara, CA) was used. A hydrophilic capillary EX-nano Inertsil CN-3 0.2mm × 150 mm × 3 µm column (GL Sciences, Tokyo, Japan) was used at 35 °C. A 1 µl sample was injected, and the flow rate was at 1.5 µl/min. A gradient elution was performed with mobile phase A (5% (v/v) acetonitrile in 0.2% acetic acid)

and mobile phase B (95% (v/v) acetonitrile in 0.2% acetic acid). The gradient duration was 40.0 min. The binary gradient elution was as follows: 0–5.0 min, 100% B; 5.0–15.0 min, 70% B; 15.0–18.0 min, 40% B; 18.0–21.0 min, 30% B; 21.0–24.0 min, 5% B; 24.0–32.0 min, 5% B; 32.0–33.0 min, 100% B; and 33.0–40.0 min, 100% B.

The validation strategy is referenced in published metabolomic studies [21-23]. The stability of the chromatography system was assessed using three selected metabolites present in all samples at 1.5 min (285.14 m/z), 13.2 min (287.14 m/z), and 28.9 min (751.76 m/z), representing the early, middle, and late stages of elution. The reproducibility (coefficient of variation [CV]) of the retention times of the metabolites in each batch was assessed.

Metabolites were analyzed using Q-Tof mass spectrometry (Micromass Q-Tof micro, Waters MS Technologies, Manchester, UK) operating in both positive and negative ionization modes. The system was controlled and data was acquired using MassLynx 4.1 software (Waters Corporation). An ESI system equipped with nano lock spray was used. For the positive ESI mode, the capillary voltage was 2800 V, the sample cone was 35 V, the extraction cone voltage was 3.0 V, the source temperature was 130 °C, and the cone gas was 80 l/h. The full scan range was from 50–1000 m/z, with a scan time of 1 s and an interscan delay of 0.1 s. The microchannel plate (MCP) detector was set at 2500 V. Other parameters were optimized for the best sensitivity and resolution. Sodium cesium iodide was used for calibration before analysis. For the negative ESI mode, the capillary voltage was −3500 V, the sample cone was 35 V, the extraction cone was 3.0 V, the source temperature was 120 °C, and the cone gas was 80 l/h. The full scan range was from 50–1000 m/z, with a scan time of 1 s and an interscan delay of 0.1 s. The MCP detector was set at 2900 V. Other parameters were optimized for the best sensitivity and resolution. Leucine encephalin was used as the lock spray calibration solution. For positive ESI, 556.6606 m/z was used for the calibration. For negative ESI, 554.6147 m/z was used. Lock spray calibration was used every 5 min. Target analysis was performed for six aqueous samples from each group using the exact mass analysis method [24] using target mass ± 0.005 m/z to quantify the ionization species of target metabolites and minimize interference for the validated analysis. In addition, the tandem mass spectrometry (MS/MS) profile of some key metabolites was compared with commercially available standards or the public database mainly from XCMS using the mentioned LC method with a collision energy profile from 20–60 eV. The sequence of control and DME samples were randomly assigned in each batch. Samples were repeatedly injected in three batches to improve the precision of the analysis.

The stability of signal intensity detected by mass spectrometry over different batches of samples was assessed using selected metabolites in the quality control (QC) samples, which were a mixture of control samples and DME samples. Each QC sample was analyzed before analyzing a batch of twelve samples. The stability of QC samples was assessed based on the reproducibility (CV) of the ion signal from all the features.

Data analysis: Comparisons of clinical data between diabetic control patients and DME patients were performed using a Student *t* test, a Mann–Whitney test, and an χ^2 test when appropriate (SPSS 15.1). For the exploratory group, the mass data from control and DME samples were processed using Markerlynx™ 4.1 (Waters UK), which used ApexTrack peak integration for chromatographic peak alignment and detection. The ion counts of each feature in the sample were normalized to the total ion intensity before the statistical analysis to minimize the variation due to injection and ionization. Multivariate analysis and orthogonal partial least square discriminant analysis (OPLS-DA) were used for marker exploration. Samples were included in the analysis if the data was within 95% Hotelling's T^2 range, had a variable importance in projection (VIP) value >2, and R^2 >0.6, Q^2 >0.5. Differentiated markers were used if p(Correlation) was above 0.4 of the P (correlation) on the S-Plot, $p \leq 0.05$ based on the Student *t* test. The fold ratio was calculated as the intensity of the mass peak of DME divided by the intensity of the mass peak of control. When metabolites were highly expressed in the DME group or not detected in the control group, the fold change was assigned as >1000 folds. However, when the metabolites were not detected in the DME group but were detected in the control group, the fold change was assigned as <0.01. The markers were further confirmed by their chromatographic retention times, comparing the accurate mass to authentic standards or a public database within 10 ppm and MS/MS fragmentation characteristics to authentic standards and metabolomics databases, such as METLIN and HMDB. Pathway analysis was performed using METLIN, KEGG, Metaboanalyst 3.0, IMPaLA, and Cytoscape 3.4. The presence of metabolite groups was validated based on samples from other diabetic patients with DME and diabetic control patients without DME.

RESULTS

There were no significant differences in age, number of patients, or gender between the DME patients and diabetic patients without DME (control) groups (Table 1). The

Table 1. Comparison of the characteristics of diabetic macular edema (DME) with diabetes mellitus (DM) undergoing cataract surgery patients.

Patient status	DME	DM	P value
Number of Patients	18	18	n/a
Gender (Female)**	6 (33%)	6 (33%)	NS
Age range*	63–88	66–87	NS
Blood glucose level(mmol/l)*	7.63±2.53	7.39±2.08	NS
BMI*	18.3±8.5	22.4±1.1	NS
Diabetics duration (year)*	5.29±6.50	3.90±3.44	NS
Systolic blood pressure (mm Hg)*	135.4±8.4	131.3±10.9	NS
Diastolic blood pressure (mm Hg)*	65.75±11.5	72.9±9.0	NS

*- p value calculated by *t* test; **- p value calculated by chi-square test; Value – mean ± standard derivation; NS – not significant (p>0.05); n/a – not applicable.

reproducibility (CV) of retention times of three markers from 24 samples at 1.6, 13.5, and 28.9 min were 0.03–1.1% (Appendix 1). The reproducibility (CV) of the signal intensity for the three selected metabolites from the QC samples in each analysis batch was from 7.5–23.0%. Over 80% of ions in the QC samples were within 30% CV.

The DME and control samples were within 95% of Hotelling's T^2 range, and the distance to the model was mostly within 0.05. This indicates that the system was stable during analysis, that the samples were homogeneous, and that the model fit the analysis (Appendix 2). Figure 1 shows that the metabolic profiles from the DME and control groups analyzed using OPLS-DA were clearly separated. The most highly separated metabolites in the S-plot were used for further analysis (Figure 2). The upper right quarter of metabolites was highly expressed in the DME group, whereas the lower left quarter showed metabolites highly expressed in the diabetic control patients without DME. The metabolites chosen for further filtering were above 0.4 and present in the flatter region in the DME group and were below −0.4 and present in the flatter region in the control group.

For hydrophilic analysis, positive ESI produced 41,245 features, whereas negative ESI produced 122 features. For hydrophobic analysis, positive ESI produced 14,466, and negative ESI produced 1940 features. Of these, 26 features passed through the filtering system. Eight groups of metabolites were grouped. These are associated with different biologic functions, such as anti-oxidation, vitamin co-factor, inflammation, neurotransmission, cellular repairing, energy production, signalling, and respiration since they involved many essential biochemical substances in the body, including fatty acids, lipids, nucleotides, peptides, amino acids, and sugars (Table 2). The highly differential expressed markers were further analyzed using Metscape (Figure 3) and

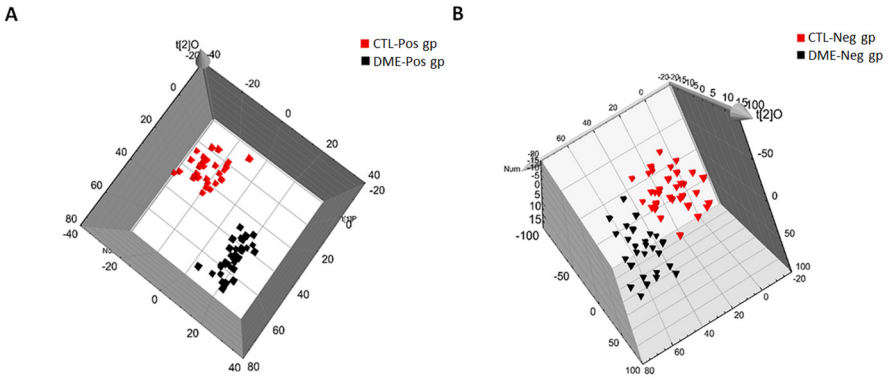

Figure 1. Score plots of aqueous humor samples from diabetic macular edema (DME; black square) and normal diabetic control patients (DM; red square) as analyzed using orthogonal partial least square discriminant analysis (OPLS-DA). Samples were analyzed using (**A**) positive electrospray ionization (ESI) and separated by an ultra-performance liquid chromatography (UPLC) nano-C18 column and (**B**) negative ESI and separated by an HPLC hydrophilic cyano (HILIC CN) micro-column (bottom).

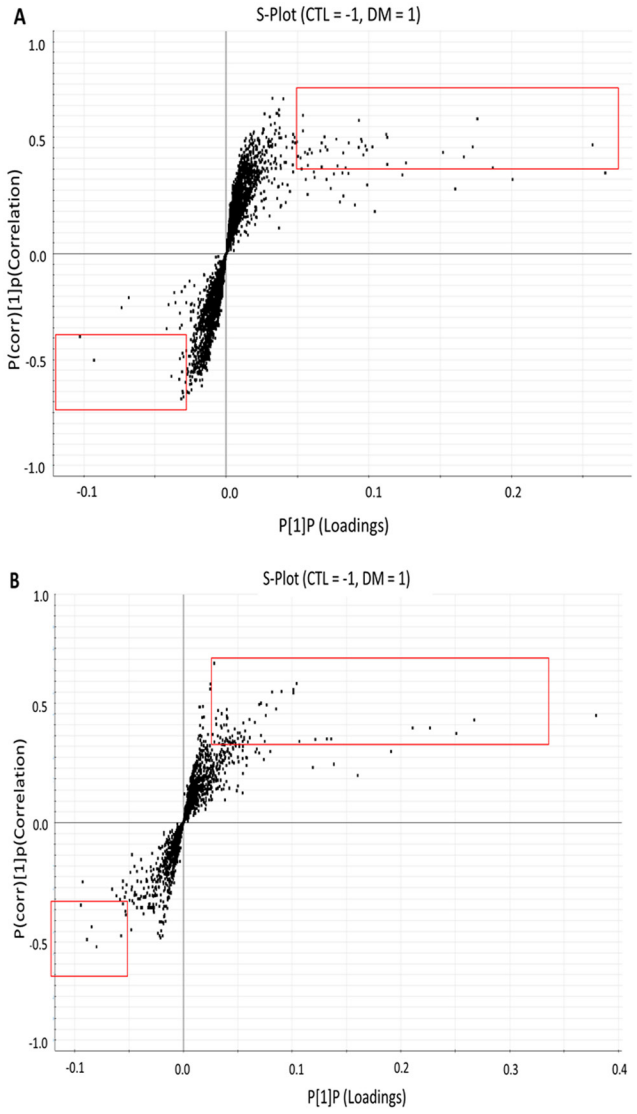

Figure 2. Diagrams of S-plot analyzed using orthogonal partial least square discriminant analysis (OPLS-DA). Metabolites obtained from diabetic macular edema (DME; upper right: 1) and normal diabetic control (DM; lower left: −1) patients analyzed using (**A**) positive electrospray ionization (ESI) separated by an ultra-performance liquid chromatography (UPLC) nano-C18 column and (**B**) negative electrospray ionization (ESI) separated by an HPLC hydrophilic cyano (HILIC CN) micro-column (bottom). A square indicates markers were included for further analysis.

Metaboanalyst (Appendix 3) and were found to be associated with pathways such as the glutathione, selenocompound, biotin, fatty acid oxidation, monoacylglycerophosphocholine, unsaturated fatty acid, sphingoid, prostaglandin, dopaminergic, cysteine, methionine, and glycolysis/gluconeogenesis biosynthesis pathways.

The final expressed key targeting metabolites were verified using targeting analysis, as shown in Table 3. Fold changes of some representative metabolites, such as dehydroascorbic acid, an antioxidant, was >1000 fold, with p=0.003; glucose was 1.2, with $p=1.2 \times 10^{-5}$; 7,8-diaminononanoate, a biotin precursor, was 2.0, with $p=1.5\times10^{-4}$, with p=2.0; 19(R)-hydroxy-PGF1α, an inflammation maker, was 1.8, with p=0.037; 5-hydroxytryptophan, a neurotransmitter, was 2.2, with $p=5.5 \times 10^{-5}$; and decanoyl-L-carnitine, associated with mitochondrial fatty acid oxidation, was 1.6, with p=0.0004. The results imply metabolic dysfunction and tissue damage. The MS/MS spectra of some targeted metabolites were comparable to commercially available standards (Appendix 4). Other metabolites were compared to results in the published literature.

DISCUSSION

In this study, we compared the metabolomic profiles of aqueous humor in DME patients with those of age- and gender-matched cataract DM patients without DME to explore the possible pathological mechanisms. It is noted that the development of cataracts is related to both age and diabetes. Metabolomic studies have shown that metabolites

Table 2. Upregulation and downregulation of metabolites, and metabolomics pathways identified by metabolomics techniques in diabetic macular edema (DME) versus diabetes mellitus (DM) undergoing cataract surgery control patients.

Metabolites group	Molecular formula	Ionization species	Experimental Ion Mass (m/z)	Molecular Mass	Proposed Pathway/ reaction	KEGG/LM No.	Regulation Fold change
Antioxidant							
Methylselenic acid*	CH4O2Se	[M+Cl]-	162.9053	127.9377	Selenocompound	map00450	2.9
Dehydroascorbic acid*	C6H6O6	[M+CH3COO]-	233.0307	174.0164	Glutathione	map00480	>1000
Glutathione amide***	C10H18N4O5S	[M+Na]+	329.0886	306.0998	Glutathione amide	R09561	0.51
Se-Adenosylselenohomocysteine***	C14H20N6O5Se	[M+H]+	433.0747	432.066	Selenoamino acid	R04939	0.74
Co-Factor							
7,8-Diaminononanoate*	C9H20N2O2	[M+Na]+	211.1454	188.1525	Biotin	map00780	2.03
Fatty acid/Lipid							
9-oxo-2E-decenoic acid*	C10H16O3	[M-H]-	183.1056	184.1099	Oxo fatty acids	FA0106	16.6
2-Undecenoic acid***	C11H20O2	[M+H]+	185.1565	184.1463	Unsaturated fatty acids	FA0103	1.6
Decanoyl-L-carnitine**	C17H33NO4	[M+CH3COO]-	374.2586	315.241	fatty acid oxidation		1.5
C16 sphingosine-1-phosphate*	C16H34NO5P	[M+CH3COO]-	410.2352	351.2175	Sphingoid	GP0105	1.54
Inflammation							
13,14-dihydro-15-keto-tetranor PGF1α*	C16H28O5	[M+H]+	301.2019	300.1937	prostaglandin	n/a	1.86
19(R)-hydroxy-PGF1α*	C20H36O6	[M-H2O-H]-	353.2348	372.2512	Prostaglandins	FA0301	2.19
Neurotransmitter							
Homovanillic acid***	C9H10O4	[M+H-H2O]+	165.0519	182.0579	Dopaminergic synapse	map04728	2.67
5-Hydroxytryptophan***	C11H12N2O3	[M+H-H2O]+	203.0869	220.0848	Serotonin		2.21
Nucleotides							
Urate-3-ribonucleoside*	C10H12N4O7	[M-H]-	299.0661	300.0706	Purine	map00240	<0.01
Uridine diphosphate (UDP)*	C9H14N2O12P2	[M+CH3COO]-	463.0174	404.0022	Pyrimidine	map00230	<0.01
Uridine 5′-diphosphoglucuronic acid*	C15H22N2O18P2	[M+H-2H2O]+	545.0188	580.0343	Amino sugar and nucleotide sugar metabolism	map00520	0.45
Peptide/Amino acid							
L-Homocysteine**	C4H9NO2S	[M+K]+	173.9989	135.0354	Cysteine and methionine	map00270	0.75
3-maleylpyruvic acid***	C7H6O6	[M+H]+	187.023	186.0164	Tyrosine	map00350	0.79
Histidinyl-Valine**	C11H18N4O3	[M+H]+	255.1484	254.1379	n/a	n/a	0.12

Metabolites group	Molecular formula	Ionization species	Experimental Ion Mass (m/z)	Molecular Mass	Proposed Pathway/ reaction	KEGG/LM No.	Regulation Fold change
Tyr-Gly-OH***	C17H16N2O7	[M+Na]+	383.0902	360.0958	n/a	n/a	2.91
Phe-Ser-OH***	C17H16N2O7	[M+Na]+	383.0878	360.0958	n/a	n/a	2.44
Ala-Tyr-OH***	C17H16N2O7	[M+Na]+	383.0876	360.0958	n/a	n/a	2.44
Asp-Phe-OH***	C18H16N2O8	[M+H]+	389.1001	388.0907	n/a	n/a	1.77
Sugar							
2-Hydroxyethylphosphonate**	C2H7O4P	[M+K]+	164.9698	126.0082	Phosphonate and phosphinate	map00440	0.59
b-Glucose*	C6H12O6	[M+Na]+	203.0503	180.0634	Glycolysis / Gluconeogenesis	map00010	1.35
Sorbitol 6-phosphate***	C6H15O9P	[M+Na]+	285.0346	262.0454	Fructose and mannose	map00051	0.66

Intensity of mass peak from DME and DM were compared by Student *t* test. The significance levels: *p<0.05, **p<0.01, ***p<0.001.

Molecular Vision 2022; 28:230-244 <http://www.molvis.org/molvis/v28/230>

associated with long-term oxidative stress and glycation, including sugars, inflammatory mediators, amino acids, and oxidized antioxidants, are present in the aqueous humor of both age-related cataracts and diabetic-related cataracts [25,26]. However, in this study, these oxidation- and glycation-related metabolites were found to be more highly expressed in the DME aqueous humor (Table 2). This indicates more severe metabolic derangements in the ocular tissue cells of DME patients compared to non-DME cataract patients. Analyses using Metaboanalyst and Metascape showed the identified metabolites in pathways and their interactions within or between different pathways (Appendix 3 and Appendix 5). The topological position of metabolites in a pathway represents biologic significance. For example, 7,8-diaminononaoate, a precursor of biotin, occupies the key position in the pathway and has a high impact on the biotin pathway. According to the interactions of the identified pathways, we suggest possible pathways that are activated in the DME eye (Figure 3). In brief, in damaged neurons, catechol, a precursor of neurotransmitters, was degraded to homovanillate and leaked out of the cell (pathway A). Glycosphingolipid from the damaged cells was degraded to sphingosine-1-phosphate (pathway E). Under hypoxia, more oxidized dehydroascorbate (DHA) was generated (pathway F) and competed with β-glucose to enter the cell through the GLUT-1 channel. DHA was reduced to ascorbic acid inside the cell by glutathione (GSH). However, in DME neurons, less GSH was produced due to lower levels of sulfur-containing compounds, Se-adenosylseleno-homocysteine, homocysteine, cysteine, and methionine, which are available (pathway C) under higher oxidative stress. In hyperglycemia, the higher level of β-glucose competed more favorably to enter the cell and was metabolized through the aldose/reductase pathway rather than sorbitol-1-phosphate (pathway B) to form more sorbitol. Lower uridine diphosphate (UDP) and UDP-glucuronate levels caused a decrease in the production of RNA, proteins, polysaccharides, and glycosphingolipids that increased cellular damage and hindered tissue repair.

The metabolic profile showed depressed antioxidant synthesis and increased antioxidant consumption, as indicated by the increase in antioxidant metabolites, such as dehydroascorbic acid and methylseleninic acid. A decrease in antioxidants, such as glutathione amide and Se-adenosylselenohomocysteine, was found in DME eyes (Table 2

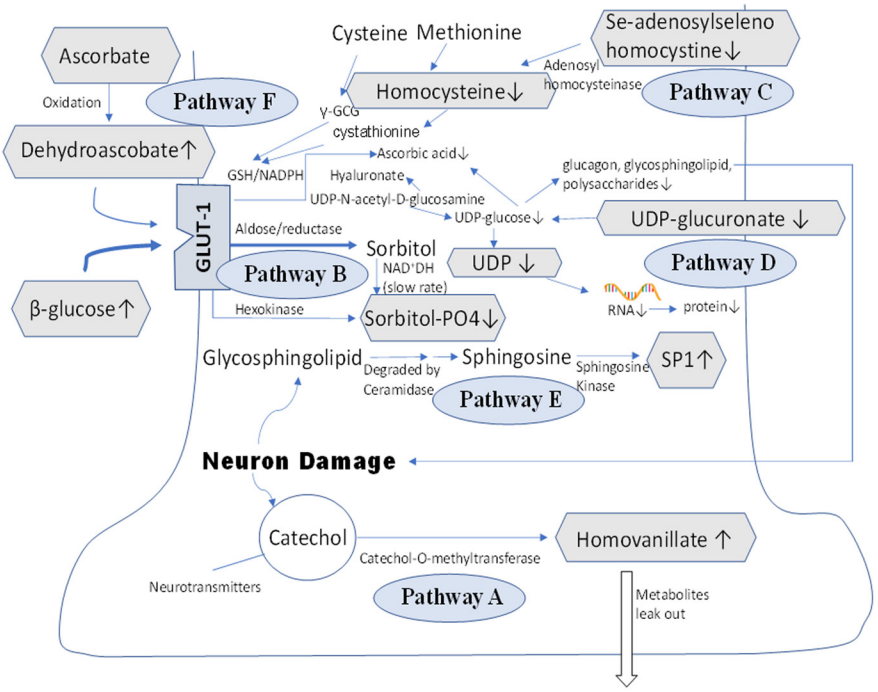

Figure 3. Pathways analyzed using Metscape. The schematic diagram summarizes different pathways and their interactions found using Metascape. The following six main pathways were found in diabetic macular edema (DME) patients: (**A**) tyrosine metabolism, (**B**) pentose phosphate, galactose, glycolysis and gluconeogenesis metabolism, (**C**) glycine, serine, alanine, threonine, methionine, cysteine, and seleno-amino acid metabolism, (**D**) pyrimidine metabolism and glycosphingolipid biosynthesis, (**E**) glycosphinolipid metabolism, and (**F**) ascorbic acid metabolism pathways. A hexagon indicates the identified metabolites with upregulation (↑) and downregulation (↓). The thicker arrow indicates higher activation of the pathway.

Table 3. Targeting analysis of key metabolites of diabetic macular edema (DME) and the diabetes mellitus (DM) control groups (n=18 for each group) using exact mass quantification.

Metabolite	Ionization species	Mass (m/z)	Fold change (DME/DM)	p-value
Methylselenic acid*	[M+Cl]-	162.9053	1.697	0.018
Homovanillic acid***	[M+H-H2O]+	165.0519	2.170	3.58439E-06
L-Homocysteine*	[M+K]+	173.9989	0.354	0.05
2-Undecenoic acid***	[M+H]+	185.1565	1.601	0.000252385
b-Glucose***	[M+Na]+	203.0503	1.172	1.20122E-05
5-Hydroxytryptophan***	[M+H-H2O]+	203.0869	2.206	5.50427E-05
7,8-Diaminononanoate***	[M+Na]+	211.1454	1.969	0.000150843
Dehydroascorbic acid**	[M+CH3COO]-	233.0307	>1000	0.003
Sorbitol-6-phosphate***	[M+Na]+	285.0346	0.662	6.81668E-05
13,14-dihydro-15-keto-tetranor PGF1α*	[M+H]+	301.2019	1.779	0.028
Glutathione amide***	[M+Na]+	329.0886	0.533	0.00035509
19(R)-hydroxy-PGF1α*	[M-H2O-H]-	353.2348	1.782	0.037
Decanoyl-L-carnitine***	[M+CH3COO]-	374.2586	1.571	0.000425371
C16 sphingosine-1-phosphate***	[M+CH3COO]-	410.2352	1.485	8.64966E-05
Se-Adenosylselenohomocysteine***	[M+H]+	433.0747	0.650	1.61927E-06
Uridine diphosphate (UDP)**	[M+CH3COO]-	463.0174	<0.01	0.007

Intensity of mass peak from DME and DM were compared by Student *t* test. The significance levels: *p<0.05, **p<0.01, ***p<0.001.

and Table 3). A low ascorbic acid level has been reported in the vitreous humor of DR [27]. Because dehydroascorbate is extensively generated in the retina and absorbed through the GLUT-1 transporter [28,29], the concentration is usually low. However, glucose can compete with GLUT-1 in hyperglycemia. A high extracellular dehydroascorbate level in DME implies more severe hyperglycemia. The lower level of Se-adenosylselenohomocysteine, which is essential for the biosynthesis of redox enzymes, may contribute to the suppression of homocysteine and other thio-amino acids, such as cysteine and methionine (Figure 3). A higher level of oxidized thio-antioxidant metabolites has also been reported in DR aqueous humor [19]. The decrease in urate-3-ribonucleoside, a precursor of uric acid, which is a major endogenous antioxidant, indicated higher oxidative stress in the DME eyes. A decrease in uric acid has been reported in severe diabetes caused by mitochondrial dysfunction [30]. Metaboanalyst showed the selenoamino acid, ascorbate acid and aldaric acid pathways were significantly changed. Metascape showed ascorbic acid was consumed to dehydroxyascorbate and homocysteine production was depressed (Figure 3 and Appendix 3). These findings provide evidence that the DME eyes were under higher oxidative stress than the DM eyes without DME.

A variety of fatty acid and lipid metabolites, such as decanoyl-L-carnitine, and an odd number of fatty acids, sphingoid metabolites, and oxidized fatty acids were highly expressed in the DME aqueous humor. Carnitine is used by cells to carry fatty acids to produce energy through transporting medium- and long-chain fatty acids into the innermost part of the mitochondria for the β-oxidation process. The accumulation of acylcarnitines implies an inefficient metabolism, which has commonly been found in insulin resistance and type 2 DM [31-33]. On the other hand, β-oxidation appeared to be a more prominent process in the retina of patients with proliferative diabetic retinopathy (PDR), as demonstrated by higher ketone bodies found in the vitreous humor [13]. The deteriorated mitochondria activity in the DME eye would further decrease the energy production of retinal cells. Accumulated acylcarnitines can also activate pro-inflammatory pathways [34], such as the cyclooxygenase-2 pathway, and the phosphorylation of JNK and ERK [35-37].

The possibility of the reduction in energy production in eyes with DME was also supported by the increase in 7,8-diaminononanoate, a precursor of biotin (Appendix 3). Increase 7,8-diaminononanoate production implies increase biotin demand during chronic inflammation. Lower biotin level supports it has been intensively consumed. Biotin is an

important regulatory factor in inflammation [38] for lymphocyte and macrophage proliferation [39,40], NF-κB activation [41], and pro-inflammatory cytokine release [40,42-44]. Biotin metabolism is also essential for cellular energy production, such as gluconeogenesis, fatty acid synthesis, fatty acid oxidation, degradation of branched-chain amino acids and odd-chain fatty acids, and leucine catabolism [45]. Its deficiency is consistent with an increase in odd-numbered fatty acids and 2-undecenoic acid and the upregulation of gluconeogenesis found in this study. The integrity of the blood–retina barrier may be deteriorated by increased odd-numbered fatty acid production [46]. The disturbance of fatty acids, amino acids, and glucose metabolism found in the plasma of DR patients has also been reported [47].

Sphingosine-1-phosphate (S1P) affects endothelial cell development and immune cell recruitment during wound healing [48-50]. A high level of S1P found in DME eyes implies that oxidation, inflammation, and edema have occurred [51]. Increased prostaglandin mediators, such as PGI_2, 19(R)-hydroxy-$PGF1_\alpha$, and 13,14-dihydro-15-keto-tetranor $PGF1_\alpha$, also indicate ocular inflammation in DME [52]. Arachidonic acid, a precursor of leukotrienes, in blood platelets was also found in higher amounts in DR patients compared to diabetic controls [53]. Because pyrimidine metabolism and glycosphingolipid biosynthesis pathways are linked, increased glycosphingolipid production may divert metabolites away from pyrimidine synthesis, which decreases cell division and subsequent tissue repair (Figure 3).

Homovanillic acid is the metabolite of the neurotransmitter dopamine and its tyrosine precursor, 5-hydroxytryptophan (5-HT). It is present mainly in amacrine and bipolar cells of the retina [54]. A high level of homovanillic acid may indicate neurodegeneration in the DME eye. Higher levels of tryptophan metabolites have also been found in the serum of DR patients [55]. The neurotransmitter metabolite acetylcholine has also been found in the vitreous humor of patients with DR [27]. Homovanillic acid is also present in the tyrosine pathway and is linked with respiratory metabolites, such as 3-maleylpyruvic acid. Decreased 3-maleylpyruvic acid may be due to metabolic pathways diverting to homovanillic acid production (Figure 3, Appendix 3). This may reflect respiratory insufficiency in the DME eye.

The extracellular matrix (ECM) plays an important role in supporting blood vessel walls, including endothelial cells [56,57]. Hyaluronan (HA), one of the major components of the ECM, has many biologic functions [58]. HA is made up of repeating units of D-glucuronic acid (GlcUA) and N-acetylglucosamine (GlcNAc) [59]. UDP-glucuronic acid is formed from glucose-1-phosphate and UDP crosslinking. The interaction of UDP and UDP-glucuronic acid produces HA. Our results showed a downregulation of UDP and UDP glucuronic acid in the ascorbate and aldarate pathways (Appendix 3), implying the DME eye has a poor ECM scaffold leading to disruption of the blood vessels in DME.

We found a higher level of di-amino acid peptides in the aqueous DME patients, implying a disruption of the blood–retina barrier, which caused macular edema. Histidinyl valine, a vasodilation peptide, was reduced in the DME eye. This would increase arterial blood pressure. High blood pressure would increase hydrostatic pressure in the microcirculation that induces fluid retention between cells, according to Starling's law [60]. Decreased homocysteine has also been found in DR [61] and severe DM [62].

Polyol pathway activation caused glucose to be reduced to sorbitol, which then forms fructose in the retina [63]. Because sorbitol does not diffuse easily through cell membranes, it accumulates in tissues, thereby causing osmotic stress and edema [64]. Low levels of sorbitol-6-phosphate and a high level of glucose found in the aqueous humor of the DME eyes support polyol pathway activation. Increased glucose may also be related to pentose and gluconeogenesis pathway activation, as shown in pathway B of Figure 3, and/or increased starch and sucrose metabolism (Appendix 3). Activation of the pentose phosphate pathway has also been reported in the plasma of DR patients, as analyzed by gas chromatography mass spectrometry (GCMS) [65].

In this study, the overexpression of various endogenous biochemical metabolites in the aqueous humor of eyes with DME revealed the metabolic derangements in DME eyes. The metabolites change was caused by more inflammation, a higher glucose level, lower anti-oxidation capacity, poor ECM integrity, higher oxidative stress, lower mitochondrial respiratory efficiency, higher vascular permeability, and more severe neurodegeneration in the DME eyes. The subsequent detrimental effects may not be compensated for by the increase in the production of protective factors, such as biotin and S1P (Figure 4).

The targeting analysis performed in this study confirmed the expression of these novel metabolites in the aqueous humor of patients with DME (Table 3). However, this study only used the metabolomic method to identify possible pathway activation and explain the pathophysiological mechanisms of DME, which is insufficient. Further works need to confirm the identified pathways with large-scale studies and need to be supported by various molecular, proteomic, and genomic technology. The biological role in DME played by the most interesting metabolites, 2-undecenoic acid, β-glucose, dehydroascorbic acid, 13,14-dihydro-15-keto-tetranor PGF1α,

19(R)-hydroxy-PGF1α, decanoyl-L-carnitine, and Se-adenosylselenohomocysteine, need to be further confirmed. Although the sample size is small, it is comparable with the sample sizes in other reports on DR [49]. Nevertheless, this is a pioneering investigation of the metabolomic study of DME.

APPENDIX 1. STABILITY OF CHROMATOGRAPHY.

To access the data, click or select the words "Appendix 1." Diagrams (a-c) showed the stability of the chromatography system. The retention times of metabolites at early (1.6 min), middle (13.5 min), and late stage (28.9 min) of the elution profile from different samples are stable. The RSD of retention time is from 0.03 – 1.1%, n=24.

APPENDIX 2. DIAGRAMS OF VARIOUS PARAMETERS:

To access the data, click or select the words "Appendix 2." i) Variable importance in projection (VIP), ii) Hotelling's T2, and iii) distance to Model. It showed examples of analysis results from positive and negative ionization analysis: (a) VIP of samples analyzed by positive electrospray (ESI) separated by nano-C18 column; (b) VIP of samples analyzed by negative charge ionization separated by hydrophilic interaction cyano (HILIC CN) column; (c) Hotelling's T2 range of samples analyzed by positive ESI separated by nano-C18 column; (d) Hotelling's T2 range of samples analyzed by negative charge ionization separated by HILIC CN column; (e) distance to Model analyzed by positive ESI separated by nano-C18 column; and (f) distance to Model analyzed by negative charge ionization separated by HILIC CN column. The green bar in (a) and (b) indicates the VIP level of each explored marker. The black color Aq_CTL_H and Aq_CTL are the aqueous humor samples from the diabetic cataract patients and the red color Aq_DM_H and Aq_DM are the aqueous humor samples from the diabetic macular edema patients in (c) and (d). The Hotelling's T2 range test verified the homogeneity of population the samples. The T2 Crit(95%) and T2 Crit(99%) indicates 95% and 99% confident levels of Hotelling's T2 range test respectively. The samples in (c) and (d) are within 95% confident level. It indicates the population in the two assays were homogeneous. The graphs in (e) and (f) also indicate the overall homogeneity of the samples.

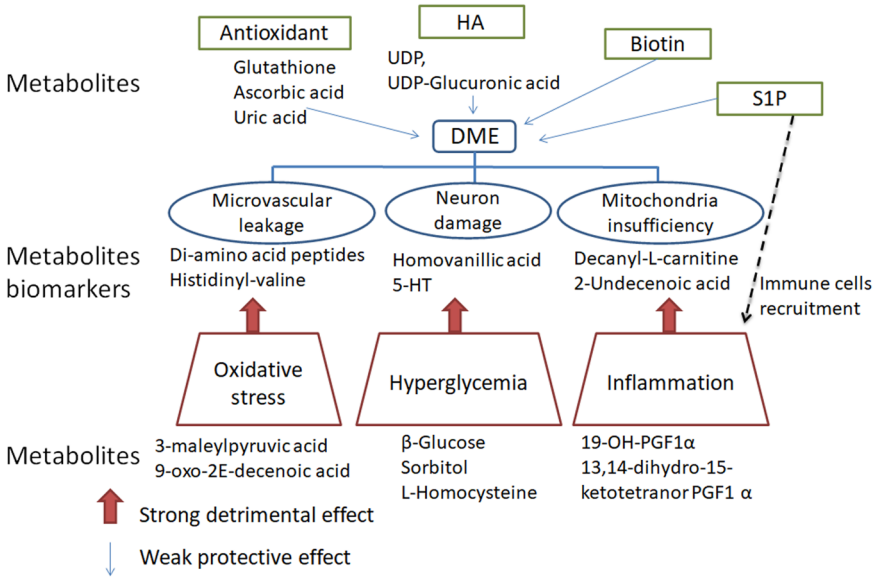

Figure 4. Summary of different proposed underlying protective and detrimental mechanisms causing diabetic macular edema (DME) in diabetic patients. The metabolites in the green boxes with thin blue arrows represent insufficiency of the system to work against oxidative stress, maintain the extracellular matrix, support energy production, and healing inflammation. These phenomena were revealed by decreased antioxidants, activated biotin pathway, elevated extracellular matrix constituents, and increased activated immune signalling sphingosine-1-phosphate pathway which involved in healing the eye of DME patients. The red box and thick arrow indicate the pathogenesis, oxidative stress, hyperglycemia, and inflammation, as implied by the associated metabolites causing the ocular tissue damage in DME patients. The blue oval indicates the involved damaged tissues/organelles found in this study, and the metabolites suggest corresponding tissue damage.

APPENDIX 3. METABOLITES ANALYZED BY METABOANALYST.

To access the data, click or select the words "Appendix 3." It shows some significant impact pathways. It shows the (a) pathways, ascorbate and aldarate, starch and sucrose, tyrosine, sulfur, selenoamino acid, and biotin, are significantly affected in diabetic macular edema (DME) patients; and metabolites present in different topological position in (b) biotin, (c) selenoamino acid, (d) ascorbate and aldarate, (e) tyrosine, and (f) starch and sucrose pathway. Red color boxes indicate the significantly identified metabolites while the blue boxes indicate the relevant metabolites in the pathway proposed by the software.

APPENDIX 4. COMPARISON OF TANDEM MASS (MS/MS) SPECTRA OF SOME KEY METABOLITES,

To access the data, click or select the words "Appendix 4." (a) 2-undecenoic acid, (b) L-homocysteine, (c) 5-OH-L-tryptophan, (d) decanoyl-L-carnitine, (e) dehydroascorbic acid, (f) homovanillic acid, (g) β-glucose, and (h)19-(R)-hydroxyPGF1α, from aqueous humor (upper) with commercial available authentic standards (lower).

APPENDIX 5. PATHWAY ANALYZED BY METSCAPE.

To access the data, click or select the words "Appendix 5." Four pathway networks were identified. The metabolites participates the pathways are (a) Tyrosine metabolism pathway, (b) pentose, galactose, glycolysis and gluconeogenesis metabolism pathway, (c) Glycine, serine, alanine, threonine, methionine, cysteine, selenoamino acid metabolism pathway, and (d) pyrimidine and glycosphingolipid biosynthesis pathway. – Big red hexagon with green outline indicates the identified input metabolites with significant level increased. Big red hexagon– small red hexagon with green outline indicates the identified input metabolites with significant level reduced.green rectangle – enzyme involved the reaction; diamond– associated reaction in the pathway; circle – gene involved in the reaction; – pink hexagon is associated metabolites deduced by Metacape during pathway exploration. The orange color text labeled in the reaction indicates a single direction reaction. The purple color text labeled in the reaction indicates a two ways reaction. Single arrow indicates single direction reaction. Double arrows at both ends indicate bidirectional reaction.

ACKNOWLEDGMENTS

Health and Medical Research Fund (Reference no.: 05162786 to Mårten Erik BRELÉN). Dr. C. P. Pang (cppang@cuhk.edu.hk) and Dr. Marten E. Brelen (marten.brelen@cuhk.edu.hk) are co-corresponding authors for this paper.

REFERENCES

1. King P, Peacock I, Donnelly R. The UK prospective diabetes study (UKPDS): clinical and therapeutic implications for type 2 diabetes. Br J Clin Pharmacol 1999; 48:643-648. [PMID: 10594464].
2. Benarous R, Sasongko MB, Qureshi S, Fenwick E, Dirani M, Wong TY, Lamoureux EL. Differential association of serum lipids with diabetic retinopathy and diabetic macular edema. Invest Ophthalmol Vis Sci 2011; 52:7464-9. [PMID: 21862642].
3. Yun JH, Park SW, Kim KJ, Bae JS, Lee EH, Paek SH, Kim SU, Ye S, Kim JH, Cho CH. Endothelial STAT3 Activation Increases Vascular Leakage Through Downregulating Tight Junction Proteins: Implications for Diabetic Retinopathy. J Cell Physiol 2017; 232:1123-34. [PMID: 27580405].
4. Schey KL, Wang ZL, Wenke J, Qi Y. Aquaporins in the eye: expression, function, and roles in ocular disease. Biochim Biophys Acta 2014; 1840:1513-23. [PMID: 24184915].
5. Byrne LC, Khalid F, Lee T, Zin EA, Greenberg KP, Visel M, Schaffer DV, Flannery JG. AAV-mediated, optogenetic ablation of Müller Glia leads to structural and functional changes in the mouse retina. PLoS One 2013; 8:e76075-[PMID: 24086689].
6. Klaassen I, Van Noorden CJ, Schlingemann RO. Molecular basis of the inner blood-retinal barrier and its breakdown in diabetic macular edema and other pathological conditions. Prog Retin Eye Res 2013; 34:19-48. [PMID: 23416119].
7. Antonetti DA, Barber AJ, Hollinger LA, Wolpert EB, Gardner TW. Vascular endothelial growth factor induces rapid phosphorylation of tight junction proteins occludin and zonula occluden 1. A potential mechanism for vascular permeability in diabetic retinopathy and tumors. J Biol Chem 1999; 274:23463-7. [PMID: 10438525].
8. Daruich A, Matet A, Moulin A, Kowalczuk L, Nicolas M, Sellam A, Rothschild PR, Omri S, Gélizé E, Jonet L, Delaunay K, De Kozak Y, Berdugo M, Zhao M, Crisanti P, Behar-Cohen F. Mechanisms of macular edema: Beyond the surface. Prog Retin Eye Res 2018; 63:20-68. [PMID: 29126927].
9. Brownlee M. The pathobiology of diabetic complications: a unifying mechanism. Diabetes 2005; 54:1615-25. [PMID: 15919781].
10. Curtis TM, Hamilton R, Yong PH, McVicar CM, Berner A, Pringle R, Uchida K, Nagai R, Brockbank S, Stitt AW. Müller glial dysfunction during diabetic retinopathy in rats is linked to accumulation of advanced glycation end-products

and advanced lipoxidation end-products. Diabetologia 2011; 54:690-8. [PMID: 21116609].

11. van der Wijk AE, Vogels IMC, van Noorden CJF, Klaassen I, Schlingemann RO. TNFα-Induced Disruption of the Blood-Retinal Barrier In Vitro Is Regulated by Intracellular 3′,5′-Cyclic Adenosine Monophosphate Levels. Invest Ophthalmol Vis Sci 2017; 58:3496-505. [PMID: 28715583].

12. Arroba AI, Valverde ÁM. Modulation of microglia in the retina: new insights into diabetic retinopathy. Acta Diabetol 2017; 54:527-33. [PMID: 28349217].

13. Barba I, Garcia-Ramírez M, Hernández C, Alonso MA, Masmiquel L, García-Dorado D, Simó R. Metabolic fingerprints of proliferative diabetic retinopathy: an 1H-NMR-based metabonomic approach using vitreous humor. Invest Ophthalmol Vis Sci 2010; 51:4416-21. [PMID: 20375324].

14. Obrosova I, Cao X, Greene DA, Stevens MJ. Diabetes-induced changes in lens antioxidant status, glucose utilization and energy metabolism: effect of DL-alpha-lipoic acid. Diabetologia 1998; 41:1442-50. [PMID: 9867211].

15. Laíns I, Gantner M, Murinello S, Lasky-Su JA, Miller JW, Friedlander M, Husain D. Metabolomics in the study of retinal health and disease. Prog Retin Eye Res 2019; 69:57-79. [PMID: 30423446].

16. Goel M, Picciani RG, Lee RK, Bhattacharya SK. Aqueous Humor Dynamics: A Review. Open Ophthalmol J 2010; 4:52-9. [PMID: 21293732].

17. Han G, Wei P, He M, He T. Glucose Metabolic Characterization of Human Aqueous Humor in Relation to Wet Age-Related Macular Degeneration. Invest Ophthalmol Vis Sci 2020; 61:49-[PMID: 32232346].

18. Kim TW, Kang JW, Ahn J, Lee EK, Cho KC, Han BNR, Hong NY, Park J, Kim KP. Proteomic analysis of the aqueous humor in age-related macular degeneration (AMD) patients. J Proteome Res 2012; 11:4034-43. [PMID: 22702841].

19. Kunikata H, Ida T, Sato K, Aizawa N, Sawa T, Tawarayama H, Murayama N, Fujii S, Akaike T, Nakazawa T. Metabolomic profiling of reactive persulfides and polysulfides in the aqueous and vitreous humors Sci Rep 2017; 7:41984-[PMID: 28169324].

20. Wei P, He M, Teng H, Han G. Metabolomic analysis of the aqueous humor from patients with central retinal vein occlusion using UHPLC-MS/MS. J Pharm Biomed Anal 2020; 188:113448-[PMID: 32622112].

21. Naz S, Vallejo M, García A, Barbas C. Method validation strategies involved in non-targeted metabolomics. J Chromatogr A 2014; 1353:99-105. [PMID: 24811151].

22. Kamleh MA, Snowden SG, Grapov D, Blackburn GJ, Watson DG, Xu N, Ståhle M. Wheelock CE. LC-MS metabolomics of psoriasis patients reveals disease severity-dependent increases in circulating amino acids that are ameliorated by anti-TNFα treatment. J Proteome Res 2015; 14:557-66. [PMID: 25361234].

23. Kenny LC, Broadhurst DI, Dunn W, Brown M, North RA, McCowan L, Roberts C, Cooper GJS, Kell DB, Baker PN. Robust early pregnancy prediction of later preeclampsia using metabolomic biomarkers. Hypertension 2010; 56:741-9. [PMID: 20837882].

24. Chu KO, Man GC, Chan KP, Chu CY, Chan TH, Pang CP, Wang CC. Determination of exogenous epigallocatechin gallate peracetate in mouse plasma using liquid chromatography with quadrupole time-of-flight mass spectrometry. J Sep Sci 2014; 37:3473-80. [PMID: 25250898].

25. Yanshole VV, Yanshole LV, Snytnikova OA, Tsentalovich YP. Quantitative metabolomic analysis of changes in the lens and aqueous humor under development of age-related nuclear cataract. Metabolomics 2019; 15:29-[PMID: 30830501].

26. Pietrowska K, Dmuchowska DA, Krasnicki P, Bujalska A, Samczuk P, Parfieniuk E, Kowalczyk T, Wojnar M, Mariak Z, Kretowski A, Ciborowski M. An exploratory LC-MS-based metabolomics study reveals differences in aqueous humor composition between diabetic and non-diabetic patients with cataract. Electrophoresis 2018; 39:1233-40. [PMID: 29292830].

27. Barba I, Garcia-Ramírez M, Hernández C, Alonso MA, Masmiquel L, García-Dorado D, Simó R. Metabolic fingerprints of proliferative diabetic retinopathy: an 1H-NMR-based metabonomic approach using vitreous humor. Invest Ophthalmol Vis Sci 2010; 51:4416-21. [PMID: 20375324].

28. Woodford BJ, Tso MO, Lam KW. Reduced and oxidized ascorbates in guinea pig retina under normal and light-exposed conditions. Invest Ophthalmol Vis Sci 1983; 24:862-7. [PMID: 6862792].

29. Hosoya K, Minamizono A, Katayama K, Terasaki T, Tomi M. Vitamin C transport in oxidized form across the rat blood-retinal barrier. Invest Ophthalmol Vis Sci 2004; 45:1232-9. [PMID: 15037592].

30. Kristal BS, Vigneau-Callahan KE, Moskowitz AJ, Matson WR. Purine catabolism: links to mitochondrial respiration and antioxidant defenses? Arch Biochem Biophys 1999; 370:22-33. [PMID: 10496973].

31. Muoio DM, Koves TR. Lipid-induced metabolic dysfunction in skeletal muscle. Novartis Found Symp 2007; 286:24-38. [PMID: 18269172].

32. Koves TR, Li P, An J, Akimoto T, Slentz D, Ilkayeva O, Dohm GL, Yan Z, Newgard CB, Muoio DM. Peroxisome proliferator-activated receptor-gamma co-activator 1alpha-mediated metabolic remodeling of skeletal myocytes mimics exercise training and reverses lipid-induced mitochondrial inefficiency. J Biol Chem 2005; 280:33588-98. [PMID: 16079133].

33. Huffman KM, Shah SH, Stevens RD, Bain JR, Muehlbauer M, Slentz CA, Tanner CJ, Kuchibhatla M, Houmard JA, Newgard CB, Kraus WE. Relationships between circulating metabolic intermediates and insulin action in overweight to obese, inactive men and women. Diabetes Care 2009; 32:1678-83. [PMID: 19502541].

34. Tilg H, Moschen AR. Inflammatory mechanisms in the regulation of insulin resistance. Mol Med 2008; 14:222-31. [PMID: 18235842].

35. Rutkowsky JM, Knotts TA, Ono-Moore KD, McCoin CS, Huang S, Schneider D, Singh S, Adams SH, Hwang DH. Acylcarnitines activate proinflammatory signaling pathways. Am J Physiol Endocrinol Metab 2014; 306:E1378-87. [PMID: 24760988].

36. Bastard JP, Maachi M, Lagathu C, Kim MJ, Caron M, Vidal H, Capeau J, Feve B. Recent advances in the relationship between obesity, inflammation, and insulin resistance. Eur Cytokine Netw 2006; 17:4-12. [PMID: 16613757].

37. Lê QH, El Alaoui M, Véricel E, Ségrestin B, Soulère L, Guichardant M, Lagarde M, Moulin P, Calzada C. Glycoxidized HDL, HDL enriched with oxidized phospholipids and HDL from diabetic patients inhibit platelet function. J Clin Endocrinol Metab 2015; 100:2006-14. [PMID: 25794249].

38. Fischer A, Munnich A, Saudubray JM, Mamas S, Coudé FX, Charpentier C, Dray F, Frézal J, Griscelli C. Biotin-responsive immunoregulatory dysfunction in multiple carboxylase deficiency. J Clin Immunol 1982; 2:35-8. [PMID: 6212592].

39. Mall GK, Chew YC, Zempleni J. Biotin requirements are lower in human Jurkat lymphoid cells but homeostatic mechanisms are similar to those of HepG2 liver cells. J Nutr 2010; 140:1086-92. [PMID: 20357078].

40. Kuroishi T, Endo Y, Muramoto K, Sugawara S. Biotin deficiency up-regulates TNF-alpha production in murine macrophages. J Leukoc Biol 2008; 83:912-20. [PMID: 18174365].

41. Rodriguez-Melendez R, Schwab LD, Zempleni J. Jurkat cells respond to biotin deficiency with increased nuclear translocation of NF-kappaB, mediating cell survival. Int J Vitam Nutr Res 2004; 74:209-16. [PMID: 15296080].

42. Wiedmann S, Eudy JD, Zempleni J. Biotin supplementation increases expression of genes encoding interferon-gamma, interleukin-1beta, and 3-methylcrotonyl-CoA carboxylase, and decreases expression of the gene encoding interleukin-4 in human peripheral blood mononuclear cells. J Nutr 2003; 133:716-9. [PMID: 12612142].

43. Aranami T, Yamamura T. Th17 Cells and autoimmune encephalomyelitis (EAE/MS). Allergol Int 2008; 57:115-20. [PMID: 18427164].

44. Kuroishi T, Kinbara M, Sato N, Tanaka Y, Nagai Y, Iwakura Y, Endo Y, Sugawara S. Biotin status affects nickel allergy via regulation of interleukin-1beta production in mice. J Nutr 2009; 139:1031-6. [PMID: 19261731].

45. Kuroishi T. Regulation of immunological and inflammatory functions by biotin. Can J Physiol Pharmacol 2015; 93:1091-6. [PMID: 26168302].

46. Mock DM, Mock NI, Johnson SB, Holman RT. Effects of biotin deficiency on plasma and tissue fatty acid composition: evidence for abnormalities in rats. Pediatr Res 1988; 24:396-403. [PMID: 3211626].

47. Li X, Luo X, Lu X, Duan J, Xu G. Metabolomics study of diabetic retinopathy using gas chromatography-mass spectrometry: a comparison of stages and subtypes diagnosed by Western and Chinese medicine. Mol Biosyst 2011; 7:2228-37. [PMID: 21559540].

48. Juarez JG, Harun N, Thien M, Welschinger R, Baraz R, Pena AD, Pitson SM, Rettig M, DiPersio JF, Bradstock KF, Bendall LJ. Sphingosine-1-phosphate facilitates trafficking of hematopoietic stem cells and their mobilization by CXCR4 antagonists in mice. Blood 2012; 119:707-16. [PMID: 22049516].

49. Aoki M, Aoki H, Ramanathan R, Hait NC, Takabe K. Sphingosine-1-Phosphate Signaling in Immune Cells and Inflammation: Roles and Therapeutic Potential. Mediators Inflamm 2016; 2016:8606878-[PMID: 26966342].

50. Goetzl EJ, Rosen H. Regulation of immunity by lysosphingolipids and their G protein-coupled receptors. J Clin Invest 2004; 114:1531-7. [PMID: 15578083].

51. Tong X, Peng H, Liu D, Ji L, Niu C, Ren J, Pan B, Hu J, Zheng L, Huang Y. High-density lipoprotein of patients with type 2 diabetes mellitus upregulates cyclooxgenase-2 expression and prostacyclin I-2 release in endothelial cells: relationship with HDL-associated sphingosine-1-phosphate. Cardiovasc Diabetol 2013; 12:27-[PMID: 23360427].

52. Wu KK, Liou JY. Cellular and molecular biology of prostacyclin synthase. Biochem Biophys Res Commun 2005; 338:45-52. [PMID: 16115610].

53. Takahashi R, Morita I, Saito Y, Ito H, Murota S. Increased arachidonic acid incorporation into platelet phospholipids in type 2 (non-insulin-dependent) diabetes. Diabetologia 1984; 26:134-7. [PMID: 6425101].

54. Ríos H, Brusco A, Pecci Saavedra J. Development of serotoninergic chick retinal neurons. Int J Dev Neurosci 1997; 15:729-38. [PMID: 9402223].

55. Munipally PK, Agraharm SG, Valavala VK, Gundae S, Turlapati NR. Evaluation of indoleamine 2,3-dioxygenase expression and kynurenine pathway metabolites levels in serum samples of diabetic retinopathy patients. Arch Physiol Biochem 2011; 117:254-8. [PMID: 22034910].

56. Davis GE, Senger DR. Endothelial extracellular matrix: biosynthesis, remodeling, and functions during vascular morphogenesis and neovessel stabilization. Circ Res 2005; 97:1093-107. [PMID: 16306453].

57. Gilkes DM, Semenza GL, Wirtz D. Hypoxia and the extracellular matrix: drivers of tumour metastasis. Nat Rev Cancer 2014; 14:430-9. [PMID: 24827502].

58. Laurent TC, Fraser JR. Hyaluronan. FASEB J 1992; 6:2397-404. [PMID: 1563592].

59. Vigetti D, Viola M, Karousou E, De Luca G, Passi A. Metabolic control of hyaluronan synthases. Matrix Biol 2014; 35:8-13. [PMID: 24134926].

60. Zhang X, Zeng H, Bao S, Wang N, Gillies MC. Diabetic macular edema: new concepts in pathophysiology and treatment. Cell Biosci 2014; 4:27-[PMID: 24955234].

61. Brazionis L, Rowley K, Sr Itsiopoulos C, Harper CA, O'Dea K. Homocysteine and diabetic retinopathy. Diabetes Care 2008; 31:50-6. [PMID: 17898092].

62. Heilman K, Zilmer M, Zilmer K, Kool P, Tillmann V. Elevated plasma adiponectin and decreased plasma homocysteine

and asymmetric dimethylarginine in children with type 1 diabetes. Scand J Clin Lab Invest 2009; 69:85-91. [PMID: 18830896].

63. Oates PJ. Polyol pathway and diabetic peripheral neuropathy. Int Rev Neurobiol 2002; 50:325-92. [PMID: 12198816].

64. Safi SZ, Qvist R, Kumar S, Batumalaie K, Ismail IS. Molecular mechanisms of diabetic retinopathy, general preventive strategies, and novel therapeutic targets. BioMed Res Int 2014; 2014:801269-[PMID: 25105142].

65. Chen L, Cheng CY, Choi HW, Ikram MK, Sabanayagam C, Tan GSW, Tian DC, Zhang L, Venkatesan G, Tai ES, Wang JJ, Mitchell P, Cheung CMG, Beuerman RW, Zhou L, Chan ECY, Wong TY. Plasma Metabonomic Profiling of Diabetic Retinopathy. Diabetes 2016; 65:1099-108. [PMID: 26822086].

Articles are provided courtesy of Emory University and the Zhongshan Ophthalmic Center, Sun Yat-sen University, P.R. China. The print version of this article was created on 19 August 2022. This reflects all typographical corrections and errata to the article through that date. Details of any changes may be found in the online version of the article.